University of Nebraska - Lincoln
DigitalCommons@University of Nebraska - Lincoln

Biological Systems Engineering: Papers and Publications | Biological Systems Engineering

12-2008

Monitoring Tissue Engineering Using Magnetic Resonance Imaging

Huihui Xu
Department of Applied Biology and Biomedical Engineering, Rose-Hulman Institute of Technology

Shadi F. Othman
University of Nebraska-Lincoln, sothman2@unl.edu

Richard L. Magin
University of Illinois at Chicago, 851 South Morgan St., Chicago, IL

Follow this and additional works at: https://digitalcommons.unl.edu/biosysengfacpub

 Part of the Biological Engineering Commons

Xu, Huihui; Othman, Shadi F.; and Magin, Richard L., "Monitoring Tissue Engineering Using Magnetic Resonance Imaging" (2008). *Biological Systems Engineering: Papers and Publications*. 54.
https://digitalcommons.unl.edu/biosysengfacpub/54

This Article is brought to you for free and open access by the Biological Systems Engineering at DigitalCommons@University of Nebraska - Lincoln. It has been accepted for inclusion in Biological Systems Engineering: Papers and Publications by an authorized administrator of DigitalCommons@University of Nebraska - Lincoln.

Published in *Journal of Bioscience and Bioengineering* 106:6 (December 2008), pp. 515-527; doi: 10.1263/jbb.106.515
Copyright © 2008 The Society for Biotechnology, Japan Published by Elsevier B.V. Used by permission.

Submitted May 19, 2008; accepted August 12, 2008; published online January 7, 2009.

REVIEW

Monitoring Tissue Engineering Using Magnetic Resonance Imaging

Huihui Xu, Department of Applied Biology and Biomedical Engineering, Rose-Hulman Institute of Technology, 5500 Wabash Avenue, Terre Haute, IN 47803, USA

Shadi F. Othman, Biological Systems Engineering, University of Nebraska–Lincoln, 233 L. W. Chase Hall, Lincoln, NE 68583, USA

Richard L. Magin, Department of Bioengineering, University of Illinois at Chicago, 851 South Morgan St., Chicago, IL 60607, USA (Corresponding author — tel 312 996-2335, fax 312 996-5921, email rmagin@uic.edu)

Abstract

Assessment of tissue regeneration is essential to optimize the stages of tissue engineering (cell proliferation, tissue development and implantation). Optical and X-ray imaging have been used in tissue engineering to provide useful information, but each has limitations: for example, poor depth penetration and radiation damage. Magnetic resonance imaging (MRI) largely overcomes these restrictions, exhibits high resolution (approximately 100 μm) and can be applied both *in vitro* and *in vivo*. Recently, MRI has been used in tissue engineering to generate spatial maps of tissue relaxation times (T_1, T_2), water diffusion coefficients, and the stiffness (shear moduli) of developing engineered tissues. In addition, through the use of paramagnetic and superparamagnetic contrast agents, MRI can quantify cell death, assess inflammation, and visualize cell trafficking and gene expression. After tissue implantation MRI can be used to observe the integration of a tissue implant with the surrounding tissues, and to check for early signs of immune rejection. In this review, we describe and evaluate the growing role of MRI in the assessment of tissue engineered constructs. First, we briefly describe the underlying principles of MRI and the expected changes in relaxation times (T_1, T_2) and the water diffusion coefficient that are the basis for MR contrast in developing tissues. Next, we describe how MRI can be applied to evaluate the tissue engineering of mesenchymal tissues (bone, cartilage, and fat). Finally, we outline how MRI can be used to monitor tissue structure, composition, and function to improve the entire tissue engineering process.

Keywords: tissue engineering, regenerative medicine, magnetic resonance imaging (MRI), elastography, organogenesis, bone, fat, cartilage, mesenchymal stem cell

Approximately one person in five in the United States will require organ replacement therapy before reaching 65 years of age (1). Physicians now treat organ failure either by surgically transplanting tissues or by replacing living tissue with mechanical/electrical devices such as artificial joints, vascular stents, or pacemakers. However, transplants rely on the availability of a compatible donor while biomechanical devices wear out and must be replaced. Tissue engineering provides a third option for patients; an option that is the focus of regenerative medicine. In regenerative medicine new sources of replacement tissues are used, sources that are not surgically transplanted, but assembled *de novo* from a three-dimensional porous scaffold imbedded with stem cells and essential growth factors. Directing this process is possible only if the tissue engineer has a clear picture of all the individual components: cells, extracellular matrix, and biochemical growth modulators. Optical and fluorescent microscopy can be used to monitor tissue growth, but even multi-photon techniques have a limited depth of field—generally up to hundreds of microns or one millimeter (2). Micro-CT solves the penetration problem but uses ionizing radiation and requires dense tissue to provide contrast (3). Much current interest is directed towards magnetic resonance imaging (MRI), which uses non-ionizing radiation and has the capability of imaging thin slices of tissue in any orientation, at any depth, and with submillimeter resolution.

As tissues grow, morphogenesis alters their physical and chemical properties. Changes in tissue hydration, macromolecular content, or water/lipid ratios, for example, are reflected in MRI as contrast in phase, diffusion, or relaxation time weighted MR images. In addition, high resolution MRI (slices less than 100 μm) can be used to characterize the structure and composition of regenerating tissues with resolution approaching that of individual cells, with the aid of high field systems above 7 T. Current applications of MRI in tissue engineering span a range from the investigation of mes-

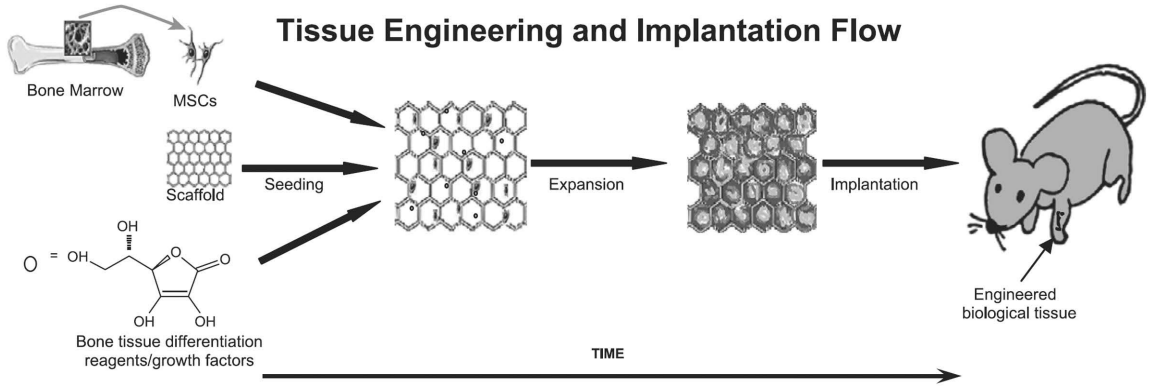

Figure 1. A flow diagram for bone tissue engineering. After isolation from bone marrow, mesenchymal stem cells (MSCs) are allowed to proliferate *in vitro*. The cells are then seeded into the biocompatible scaffold along with growth and differentiation factors (for example, β-glycerophosphate and ascorbic acid). The cells continue to grow and differentiate in an incubator or bioreactor. Upon maturity, the engineered tissue is transplanted into the animal or patient.

enchymal stem cell differentiation in culture and bulk cell expansion in bioreactors to studies in whole animals monitoring the growth of implanted bone, fat, or cartilage tissues. In order to better understand the role of MRI in tissue engineering and regenerative medicine, this review will: (i) describe the physical basis for MR contrast in developing tissues, (ii) highlight recent MRI studies of tissue engineered constructs, and (iii) outline new areas for future research and development.

Principles of tissue engineering

Tissue engineering seeks to create biological substitutes that restore, replace, or regenerate defective tissues and their function (4, 5). Successful tissue engineering requires healthy expandable cells, a porous biocompatible scaffold, biochemical growth factors, and a favorable physiological environment for tissue regeneration (6, 7). Cell sources, based on their origin, fall into three categories: autologous cells from the patient, allogeneic cells from another human donor, and xenogeneic cells from other species. Each cell source ultimately is derived from either embryonic stem cells or adult differentiated stem cells (4). Differentiated adult stem cells have the shortcoming that only a limited number of cells can be harvested from the patient, and harvesting cells causes trauma and tissue damage. These shortcomings have limited the clinical application of adult differentiated stem cells (8). On the other hand, embryonic stem cells, with proper induction, can differentiate into many tissues (mesenchymal stem cells, for example, into fat, bone, cartilage, muscle, ligament, tendon, and marrow stroma), and following *in vitro* culture and expansion can potentially provide an unlimited supply of cells for tissue transplantation. Current medical practice could use engineered tissues to treat a variety of diseases (for example, skin ulcers, joint defects, diabetes, cardiac valve failure, osteogenic tissue loss, and liver disease) (9, 10). However, before clinicians can apply engineered-tissues in regenerative medicine, the ethical and practical issues of human embryonic stem cells must be resolved, and the procedures for stem cell collection, expansion, differentiation and implantation must be perfected. In this paper we will show how magnetic resonance imaging (MRI) can be used to enhance tissue engineering through improved monitoring of cell growth and tissue development.

The strategy for using mesenchymal stem cells in tissue engineering is illustrated in Figure 1 for a bone replacement implant in a mouse. Following the successful collection of cells from donor bone marrow, the cells are expanded in cell culture and either compacted into a pellet or seeded into an artificial scaffold. Scaffolds are typically fabricated from natural-derived (for example, agarose, alginate, or collagen) or synthetic biomaterials (for example, polymers such as polyglycolic acid or hydrogels). The scaffold provides a bioactive framework for cell proliferation and differentiation. Scaffolds must have a high ratio of cell accessible space to total volume (diffusivity, porosity), with pore sizes greater than 10 microns to facilitate cell seeding and the diffusion of nutrients. In addition, the scaffold should exhibit sufficient mechanical strength to support the surrounding tissues, initially at the time of transplantation, and subsequently for the duration of the healing process. Finally, proper tissue development requires biodegradability of the scaffold and the timely application of tissue differentiation and growth stimulation factors. This entire process typically begins with cells growing in culture or in a specially designed bioreactor (for a period of weeks) and then proceeds in the animal or patient for months after implantation (11). In order to ensure optimal growth, the tissue engineer needs regular feedback about the structure, composition, and strength of the developing tissues. In the following sections, we describe how such information can be acquired using MRI for tissue engineered bone, cartilage and fat, but first we will summarize the basic principles underlying MRI and the key parameters that affect image quality, resolution and contrast.

Principles underlying image contrast in MRI

MRI is a sensitive method for visualizing structural and functional changes in biological tissues (12). For example, as tissues develop, die, or regenerate, the local environment of the tissue water—the source of the MR signal—changes. Such changes are reflected in MR images through local variations in the amount of tissue water, its physical state (e.g., freely diffusing or protein bound), and its nuclear magnetic

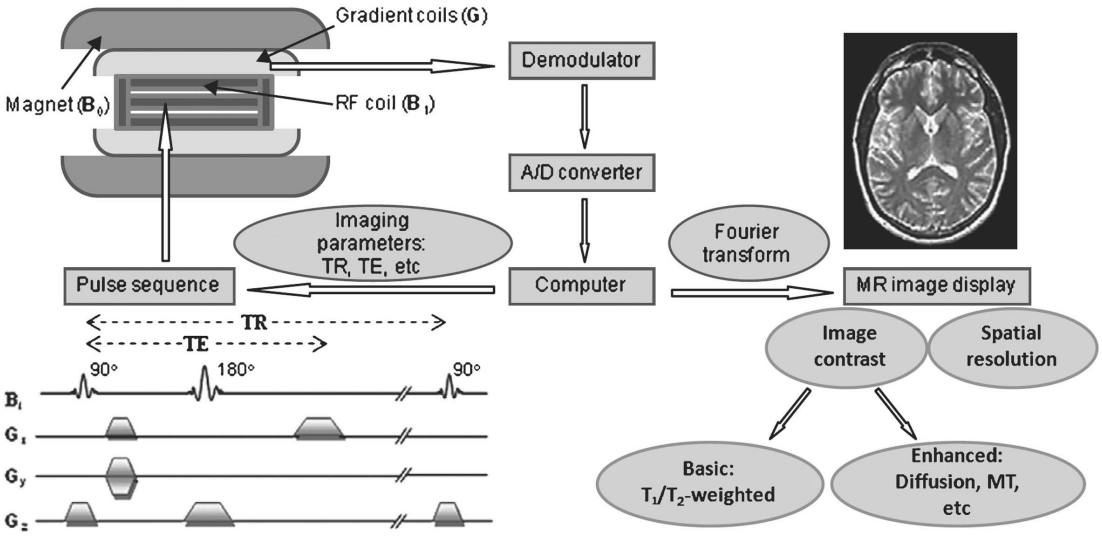

Figure 2. The block diagram of a typical MRI system with the components, pulse sequence and image display highlighted. When an animal, human or tissue sample is placed in a magnetic field (B_0), the magnetic moment of the protons in the nucleus of the hydrogen atoms of the water precess at a frequency dependent upon the strength of the magnetic field, $f_0 = \gamma\beta_0/2\pi$ where $\gamma/2\pi$ = 42.57 MHz/Tesla for hydrogen; f_0 for protons is typically in the range of 50–500 MHz. The magnetic moments align in a direction parallel to the main field establishing a net magnetization in the tissue water. A radio frequency (RF) coil produces a B_1 field that changes the direction of the magnetization in a manner prescribed by the pulse sequence (for example, 90° and 180°). Following the RF pulses, the radio frequency coil detects the return of the magnetization to thermal equilibrium. Spatial localization is generated with the use of the gradient coils (G_x, G_y, G_z). Variation of the repetition time (TR) and the echo time (TE) in the MR pulse sequence provides the basis for different contrast mechanisms. For example, a long TR and a short TE will produce a T_1 weighted image based on the MR properties of the imaged sample. Other conditions can generate T_2, proton density or diffusion weighted images. The MR signal is acquired as a complex quantity (magnitude and phase). The magnitude is sufficient to depict anatomical features, measure tissue relaxation times or estimate the apparent water diffusion coefficient, while the phase can be used to measure blood flow, tissue temperature and tissue stiffness.

resonance (NMR) relaxation times (T_1 and T_2). The dynamics of these changes in tissue water are captured in MRI by the Bloch equation: a phenomenological equation describing the physics of magnetic moments—such as the magnetic moment of the water proton—as a precessional gyroscopic motion in the presence of exponential damping (T_1 and T_2), perturbing magnetic fields (the fixed, B_0 and the time-varying radiofrequency, B_1), and magnetic field gradients (G_x, G_y, G_z). The reader is directed to the book "Magnetic resonance imaging: physical principles and applications" by Kuperman (13) for a concise description of the physics underlying the Bloch equation and for a discussion of the prevailing techniques used to acquire and display MR images. Here we will only illustrate the process diagrammatically (Figure 2) via the connections between the MRI imaging system, the image acquisition pulse sequence, and the reconstructed MRI image/display. MRI begins with selection of the pulse sequence parameters in an imaging protocol (Figure 2) that specify the field of view, signal-to-noise ratio and spatial resolution. The pulse repetition time, TR, defines the time period over which the tissue water can recover its observable magnetization; the echo time, TE, is the time period after the initial radio frequency pulse when the signal (echo) is recorded; and the magnetic field gradient pulses (G_x, G_y, G_z) give spatial localization for the NMR signal in the sample. For the spin echo sequence described in Figure 2, the signal intensity is proportional to the local water concentration multiplied by the exponential decay expression $(1\text{-}e^{-TR/T_1})e^{-TE/T_2}$. Thus, changes in tissue during growth that affect the amount of water or change its T_1 or T_2, for fixed values of TR and TE, will alter the magnitude and phase of the detected MR signal. Regions of the image exhibiting different signal intensities are revealed as contrast in the image.

In a digital MR image, the field of view (FOV) for single slice can be decomposed into individual picture elements (pixels) that determine the resolution of the image. The relationship between pixels and FOV in the x and the y directions, for example, is simply: $FOV_x = N_x\Delta x$ and $FOV_y = N_y\Delta y$, where N_x and N_y are typically 128 or 256. Acquisition of an MR image involves sampling the detected NMR signal for each of the slices of the object under study. The mathematics of sampling requires the sampling intervals to be less than two times the reciprocal of maximum frequency (Nyquist sampling criterion). This constraint gives the following simple relationships between MR imaging parameters, and the resolution for rectilinear sampling (13) for the spin echo pulse sequence shown in Figure 2.

$$\Delta x = FOV_x \div N_x = 2\pi \div N_x \gamma G_x T_{acq} \quad (1)$$

$$\Delta y = FOV_y \div N_y = 2\pi \div N_y \gamma G_y T_{pe} \quad (2)$$

In these expressions $\gamma/2\pi$ is the gyromagnetic ratio (42.58 MHz/T for water protons), G_x and G_y are the magnitude of the x (read) and y (phase) encoding gradients (typically, 1–200 G/cm), and T_{acq} and T_{pe} are the duration of the acquisition window (typically 1–10 ms) and the phase encoding gradient (typically, ≤5 ms), respectively. From these equations it follows that stronger gradients (G_x, G_y, G_z) improve the achievable resolution (typically 50 to 500 microns). The slice location and thickness are determined by modulation of the transmitted radio frequency pulses (B_1 in Figure 2). For the typical sinc pulse modulation the slice thickness is given

by

$$\Delta z = 4\pi \div \gamma G_z \tau_p \quad (3)$$

where τ_p is the duration of the 90° B_1 pulse (typically 5 ms).

The signal-to-noise ratio (SNR) associated with MR imaging can be summarized by the expression

$$\mathrm{SNR} \propto B_0^2 V_s N \quad (4)$$

where B_0 is the strength of static magnetic field, V_s is the volume of the sample and N is the number of acquisitions (14). High field MRI (3 Tesla and above) thus directly improves the SNR and allows faster imaging without compromising the resolution. The ability to distinguish individual pixels in a given MR image is known as contrast. Since image noise often limits the achievable contrast, a figure of merit used to characterize image contrast is the contrast to noise ratio (CNR), defined for two tissue regions A and B as

$$CNR = (SNR_A - SNR_B) \div Noise \quad (5)$$

Contrast, thus depends on increasing the relative difference between the signal intensities of two adjacent regions of an image and reducing the overall noise level. The noise can be estimated from the expression

$$Noise = (4k_B T \Delta f R)^{1/2} \quad (6)$$

where k_B is the Boltzman's constant, T is the absolute temperature, Δf is the detector's frequency bandwidth and R is the overall resistance of the loaded RF coil.

Optimal tissue contrast relies on selection of an appropriate imaging strategy to highlight the intrinsic differences between various tissues. Basic tissue contrast arises from the relative abundance of the hydrogen nuclei under investigation, that is, water content, and the two relaxation times: spin-lattice relaxation T_1 and spin-spin relaxation T_2 (12). Advanced contrast methods include injection of paramagnetic contrast agents such as Gd-DTPA, and the use of MR techniques that are sensitive to water diffusion in the tissue (13, 14). An example of current animal work using contrast agents is the study by Ko and coworkers (15), where the investigators demonstrated that MRI could be used to monitor and track transplanted cells *in vivo*. In this preliminary study human bone marrow-derived MSCs were labeled with super paramagnetic iron oxide, a strong T_2 contrast agent. After the cells were embedded in a gelatin sponge the construct was implanted subcutaneously at the right proximal thigh of a 6 week-old nude mouse. MR images confirmed that cell labeling could be observed in living animals; a critical first step in establishing *in vivo* monitoring.

Methods to Enhance Image Contrast in MRI

Water, the principal source of the signal detected in MRI, occupies multiple tissue compartments (for example, intravascular, extracellular, intracellular) where diffusion and tissue heterogeneity modulate water's complex interactions with proteins, macromolecules and membranes. Local changes in the bulk water distribution and the compartmental T_1 and T_2 relaxation measurements do not always give specific measures of tissue complexity; hence, other techniques are needed to provide a complete picture of the changing dynamics occurring during tissue growth. Diffusion weighted MRI, magnetization transfer (MT) contrast and $T_{1\rho}$ relaxation, for example, are MR techniques that can provide additional information about tissue structure and composition. In addition, chemical shift imaging and MRI-based tissue elastography can be used to measure the chemical and physical properties, respectively, of individual tissue compartments. Here we describe the basic principles underlying these advanced contrast methods in MRI. Additional details can be found in the cited references.

Diffusion contrast — When implanted cells proliferate and become organized into tissue the overall diffusion of water decreases because the molecules encounter additional physical barriers (16). Diffusion weighted MRI provides a means to identify the emerging tissue structure through the reduction of the apparent diffusion coefficient. The mechanism underlying diffusion weighted imaging is the application of a sequence of two short duration (δ) gradient pulses of opposite polarity that are separated by a delay time (Δ). In the absence of diffusion the two pulses induce small phase shifts that compensate for each other, but when diffusion occurs the cancellation is incomplete and additional signal attenuation arises; typically the signal is attenuated according to e^{-bD}, where $b = (\gamma G_z \delta)2\Delta$ for $\Delta >> \delta$ and b is determined from the area ($G_z\delta$) and separation (Δ) of the applied gradient pulses. By stepping b over a range from 100 to 2000 s/mm^2 or higher the exponential signal decay can be plotted and the apparent diffusion coefficient, D, determined for the tissue (16). In isotropic, but heterogeneous tissue, D changes with location but is independent of direction; hence, a single value of D is sufficient to characterize the diffusion of each voxel. When the tissue environment is anisotropic, however, such as in white matter of the brain or in articular cartilage, D is described by a 3×3 matrix or diffusion tensor (16). Diffusion weighted and diffusion tensor imaging are typically conducted at submillimeter resolution, providing spatial maps of the apparent water diffusion coefficient. In diffusion weighted MRI the diffusion data are often presented as diffusion ellipsoids, which can be calculated for each voxel, such that by their eccentricity and orientation the paths of preferred diffusion can be identified (16).

Magnetization transfer contrast — Magnetization transfer contrast depends on the exchange of magnetization between the protons (H nuclei) of free water and water bound to proteins and other macromolecules (17). In this technique, an off resonance radio frequency pulse is applied, which ideally eliminates the signal associated with macromolecular water. Subsequent interaction and exchange between the two water pools give a signal that reflects the distribution of macromolecules in the tissue—via the magnetization transfer ratio (MTR). Magnetization transfer is currently used in MR angiography to attenuate the signal from brain tissue and to improve contrast between blood vessels and surrounding tissue (18). The MTR is also sensitive to the structural changes that occur in cancer, arthritis and multiple sclerosis. For example, in a study by Brochet and Dousset (19), a reduction

in the MTR was found in demylinated lesions, and that decrease was proportional to the level of myelin loss. In cartilage tissue engineering we would anticipate an increase in MTR with the incorporation of collagen and proteoglycans in developing cartilage (20).

T_{1r} contrast — T_{1r} is a relaxation parameter that is sensitive to molecular processes occurring at a much lower frequency range than those associated with T_1 relaxation (kHz instead of MHz). T_{1r} measurements are essentially T_1 measurements performed while the radio frequency B_1 pulse is left on for the entire relaxation period. T_{1r} values reflect the macromolecular content of the tissue more strongly than T_1 relaxation times. T_{1r} contrast arises, for example, when the collagen matrix is disrupted in diseased cartilage. In a recent study of cartilage, for example, a statistically significant change in T_{1r} was observed between native and enzymatically treated cartilage (21). Changes of T_{1r} were also observed in proteoglycan-depleted cartilage, indicating T_{1r} sensitivity to proteoglycan content (22).

Chemical shift — Chemical shift imaging separates signals from each chemical component in a tissue (23). The separation is based on the small difference between the individual resonance frequencies for hydrogen atoms associated with water or with lipids. For example, between fat lipids and water, there is a frequency shift of approximately 450 Hz (at 3.0 T). By applying frequency selective radio frequency pulses it is possible to excite individual hydrogen nuclei in tissue. Since the methylene ($-CH_2-$) group is typically associated with fat while the surrounding water contain free and bound water the two pools can be separated by their characteristic frequencies. Thus, chemical shift imaging provides separate images for each tissue component. Chemical shift imaging can also be used either to suppress the fat signal in MRI or to highlight the development of adipose tissue in tissue engineering.

Magnetic resonance elastography — Stiffness or elasticity is an intrinsic mechanical property of biological tissues that changes in disease, with recovery from injury, and as tissue regrows or regenerates. Magnetic resonance elastography provides maps of tissue stiffness from the analysis of a phase contrast MR image acquired while applying a low frequency mechanical shear wave (typically with amplitudes of less than 100 μm and frequencies of 100–1000 Hz). The periodic vibrations are synchronized with the MR image acquisition (24) and motion encoding gradients stepped in sequence to provide shear wave motion images that can be analyzed to extract tissue elasticity maps (stiffness and viscosity). Bulk elastic parameter data can be used to assess developing pathology and tissue regeneration. For example, in the recent study by Cheung and associates, MR elastography was used to observe changes in the shear modulus of plantar fat pads in diabetics (25).

Bone Tissue Engineering

Trauma, osteoporosis, and cancer lead to over two million cases of bone injury or loss in the United States each year (26). Natural bone healing following injury or disease is the preferred option to overcome osteogenic tissue loss and bone damage. However, since bone has a limited capability to regenerate and remodel, it is often the case that the surgeon will need to implant synthetic materials or bone grafts at the site of injury. Approximately one million cases of bone grafting are performed each year in the United States to treat non-union following fracture, at an estimated cost of over $3 billion per year (26). Both autologous and allogeneic bone grafts are used clinically as bone substitutes; however, the availability of compatible bone grafts is limited because harvesting bone is painful and the procedure carries the risk of infection. Therefore, alternative tissue sources are needed.

Bone is a dense connective tissue with a strong calcified outer layer (cortical bone) that comprises more than three fourths of the bone mass. Cortical bone has a relatively low porosity, ranging from 5% to 10% (porosity is a measure of the available fluid volume of bone, and can be determined from the ratio of dry to fresh, wet bone weight). The soft inner spaces of bone (usually described as cancellous or trabecular bone) form the remaining one fourth of the bone mass. Cancellous bone has a high porosity (ranging from 60% to 90%) and contains the bone marrow, which consists of blood stem cells, adipose cells, osteoblasts, and osteocytes. Osteoblasts are essential for the deposition and mineralization of the extracellular matrix of new bone while osteocytes are the supporters for bone matrix calcification. Specific growth factors and proteins, mainly residing in the extracellular matrix of bone, are responsible for regulating cellular activity and stimulating the intracellular environment. The factors and proteins that the tissue engineer must control include transforming growth factor-beta (TGF-beta), insulin-like growth factors (IGF) I and II, fibroblast growth factor (FGF), and bone morphogenetic proteins (BMPs) (27).

Replacing the natural repair processes in bone is the goal of bone tissue engineering. To achieve this goal a source of bone forming cells must be found and a means of physically supporting these cells in a structural scaffold developed. Bone marrow stromal cells, also called mesenchymal stem cells (MSCs), can be stimulated to differentiate into osteoblasts, chondrocytes and adipocytes, and thus they can provide a potential source for bone progenitor cells (28). Biocompatible scaffolds of bone tissue engineering should be mechanically stiff, porous, and moldable (28). Commercially available bone scaffolds vary in composition, spanning a range that includes ceramics, metals, polymers, and natural materials (26). Natural biodegradable polymers are often used because they integrate most easily with surrounding tissues (28). Researchers have been successful using MSCs to regenerate bone in bioreactors, in animal models and in clinical trials. X-ray and micro-CT imaging techniques are most suitable for viewing solid bone growth, but early bone tissue development can be monitored using conventional MRI and the new ultra short TE methods, under development (29).

MRI of bone — Cortical bone is not visible in conventional MRI. Bone appears dark because of the relatively low number of hydrogen atoms in the bone mineral and the very short T_2 relaxation time of the solid material: cortical bone has an average T_2 of 250–500 μs (30). Bone can be imaged, using ul-

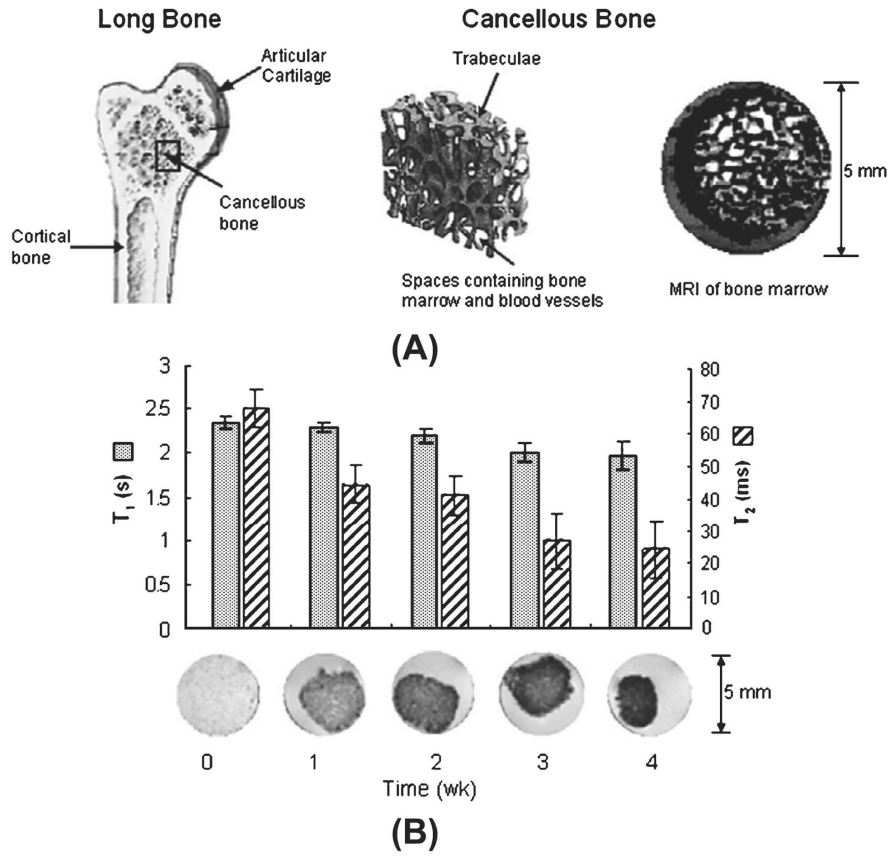

Figure 3. (A) An illustration of the anatomical structure of a long and cancellous bone, and a T_1-weighted axial MR image (field strength = 11.7 T; spin echo sequence TR/TE = 500 ms/7 ms, slice 1 mm) through a cylindrical osteochondral plug excised from the distal femoral condyle. (B) T_1/T_2 bar chart and high resolution axial MR images for tissue engineered bone (33) over a 4-week period. The relaxation time data show that T_2 is a good marker for studying the development of the construct while T_1 is less sensitive. The high resolution images were acquired with acquisition parameters: TR = 1 s; TE = 30 ms; slice thickness = 0.5 mm; field of view (FOV) = 0.8 cm × 0.8 cm; in-plane resolution = 62.5 μm × 62.5 μm; and number of averages N = 8. The MR images show the consolidation of the construct (diameter decreases by 50%) and a fall in overall signal intensity with the incubation time. Relaxation times are represented by average ± std (sample size n = 7).

trafast MR imaging sequences that capture the data quickly (in less than 1 ms after excitation), but such techniques are not widely available and require special high speed imaging hardware (30, 31). Therefore, the predominant features visible in MR images of bone reside in the bone marrow (Figure 3). Contrast in the bone marrow reflects the micro-architecture and its fat/water composition. However, special care must be taken when viewing the interface between the marrow and the surrounding solid bone tissue where the transition between the marrow and cortical bone can induce magnetic field artifacts and distort the MR image.

Progress in monitoring tissue-engineered bone *in vitro* — X-ray micro-tomography (micro-CT) of cortical bone exhibits high resolution and contrast; however, the X-ray contrast is less apparent in the marrow and in newly formed bone prior to mineralization. Thus, MRI, with its superior soft tissue contrast, can be expected to provide greater detail in images of the beginning stages of bone growth. Such results were in fact observed in an *in vitro* study comparing micro-CT and 9.4 T MRI by Washburn and coworkers (32). In this study of bone formation a porous polyethylmethacrylate scaffold was seeded with primary chick osteoblasts. Growth was assessed over an 8 week period by following the loss of MR signal in proton density MR images and the appearance of solid bone contrast in the micro-CT images. A similar progressive decrease in the MR signal was observed by Xu and coworkers (33) in a 4-week study of osteogenesis by MSCs embedded in a gelatin scaffold. Xu used 11.7 T MRI to monitor bone formation and found a linear relationship between the concentration of bone minerals, such as calcium, and the T_1 and T_2 relaxation times. In Xu's study the T_2 was reduced by over 50% as the bone developed (Figure 3); a T_2 decrease similar to that observed by Washburn and coworkers (32). In both the Xu and the Washburn studies the observed decrease in relaxation times correlated with bone mineral deposition—as measured by histological analysis (calcium composition and alkaline phosphatase activity). Also, both groups reported that the apparent diffusion coefficient decreased, likely reflecting the increase in structure (interfaces and barriers to diffusion) of the engineered bone tissue. On the other hand, in another bone growth study using MR microscopy at 9.4 T Chesnick and associates (34) found that the T_2 values increased. This research monitored mineralization in a hollow fiber bioreactor seeded with embryonic chick osteoblasts. Proton density MR images as well as T_2 relaxation time and magnetization transfer ratio maps were obtained with a 78 μm resolution for 1 mm slices. The magnetization transfer ratio was found to change with mineralization

in bone constructs, that is, higher values were observed in the mineralized zone and non-uniform but lower values in the superficial region. These results illustrate the complexity of monitoring bone formation in different systems, hence the need for MR microimaging, quantitative parameter measurements and histological controls.

An important measure of bone development is mechanical strength. MR elastography is able to assess tensile strength through measurements of bone stiffness and elasticity. In a study of bone development by Othman and coworkers (35), MR elastography was used to characterize the early stages of bone formation in gelatin scaffolds embedded with MSCs. This study measured the shear stiffness of developing bone over a two week period. Compared with controls, a three- to fourfold increase in shear stiffness was reported during the initial stages of growth: 11.88±0.4 kPa at week 1 and 15.8±0.5 kPa at week 2 for the treated groups (compared with 4.1±0.3 kPa at week 1, and 3.6±0.4 kPa at week 2 for controls). Othman's study also revealed a non-uniform growth of bone components within the sample, and considerable variation of the MR parameters from region to region. Such results could reflect either non-uniform seeding of stem cells in the scaffold or a problem with the distribution of nutrients and growth factors.

Progress in monitoring tissue-engineered bone *in vivo* — As *in vitro* tissue engineering methods are perfected there will be an increasing need for *in vivo* monitoring of implants, first in animals and later in human clinical trials. In an animal study by Hartmen and associates (36), MRI was used to assess the growth and development of bone. Using a rat model, Hartmen employed high resolution MRI at 7.1 T to monitor ectopic bone formation over a 7-week period. The post-implantation MR and X-ray images, and histological results, confirmed that MRI could detect small changes in bone growth (0.5 mm in diameter), as well as display the complete 3D shape of the newly formed bone. In another bone growth study using an athymic mouse model, Potter and coworkers (20) used MR microscopy to evaluate the growth and development of tissue engineered phalange constructs. MR microscopy images at week 38 showed the engineered specimen to be about 3 mm longer and more heavily mineralized than controls. In this study, an inverse linear relationship was found between mineral concentration measured by X-ray micro-CT and tissue hydration as measured by MR microscopy at 9.4 T. Such animal studies show that MRI can be used to monitor the progressive changes of engineered bone that occur over a period of months and that MRI can serve as a complement to micro-CT (37).

Cartilage Tissue Engineering

A major degenerative disease of articular cartilage is osteoarthritis. Osteoarthritis affects approximately 70 million people in the United States and is the leading cause of chronic disabilities in people over 50 years of age (38). The cost of treating arthritis and related conditions in the United States is over 65 billion dollars per year (39). Current cartilage restoration therapies rely on either tissue grafts or engineered cartilage substitutes. Replacement tissue grafts (autografts or allografts) have a success rate of approximately 70% after two to five years (40). However, cartilage grafts have the common shortcomings of all transplant therapies: donor availability, donor site morbidity (due to excessive tissue loss) and the possibility of pathogen transmission (39). Engineered cartilage substitutes, when fully developed, have the potential to overcome these limitations.

Articular cartilage is a thin heterogeneous tissue with a thickness typically less than 2 mm that coats skeletal joint surfaces. Cartilage consists of collagen—mostly in the form of type II collagen—and proteoglycans. Articular cartilage has four distinct zones: the superficial zone with collagen fibrils oriented along the cartilage surface (approximately 5–10% of thickness in humans), the transitional zone with randomly oriented collagen (approximately 40–45% of thickness), the radial zone with radially oriented collagen (approximately 40–45% of thickness), and the deepest calcified zone, which has little collagen and acts as a transition region between the soft hyaline cartilage and the stiffer subchondral bone (approximately 5–10% of thickness). Each of the four zones has different biomechanical properties that are consistent with their structure and function (41).

Cartilage tissue engineering has the goal of reestablishing the natural state in damaged cartilage. The process first involves introducing progenitor cells into the injured site, with or without a scaffold. The best source of cells for cartilage repair is an area of active investigation; both chondrocytes and stem cells are widely used in cartilage tissue engineering. The primary advantage of chondrocytes is that they immediately begin to secrete cartilage-specific extracellular matrix components and thus can more rapidly form cartilage-like tissue (<2 months) (39, 40). In orthopedic clinics, implantation of a suspension of cultured autologous chondrocytes is becoming an established technique for the treatment of joint surface defects of the knee. However, despite promising clinical results, the use of chondrocytes has some limitations, principally due to the low expandability of chondrocytes and the complexity of biological responses in the periosteum (8). A large number of donor cells are needed to repair a large cartilage defect, but these cells are often not available. In contrast, MSCs are relatively easy to harvest, and are expandable from small quantities *in vitro* in cell culture, and can be induced to differentiate into chondrogenic cells (39). Therefore, chondrogenic cells derived from MSCs are a promising choice for developing cartilage regeneration.

Even though cartilage is a relatively simple tissue with a low cell density, limited cell diversity and the absence of vascular structure or nerve supply, so far, tissue engineering techniques have not succeeded in producing an implant capable of functioning *in vivo* at the joint surface (42). One problem facing tissue engineers is the selection of an appropriate biological scaffold. Natural and synthetic scaffolds are available in various physical forms, and compared with natural materials, synthetic scaffolds are easily mass-produced and free from the risks associated with pathogen transmission. Solid polymers such as polyglycolic acid or composites, such as, hyaluronan-gelatin have also been successfully applied in chondrogenesis (43, 44). In addition, other groups are exploring hydrogels (highly hydrated polymeric systems with tissue-like water content) as a framework in which to encapsulate cells (45). To date, naturally derived collagen, the major structural component of cartilage, has received the most attention, largely be-

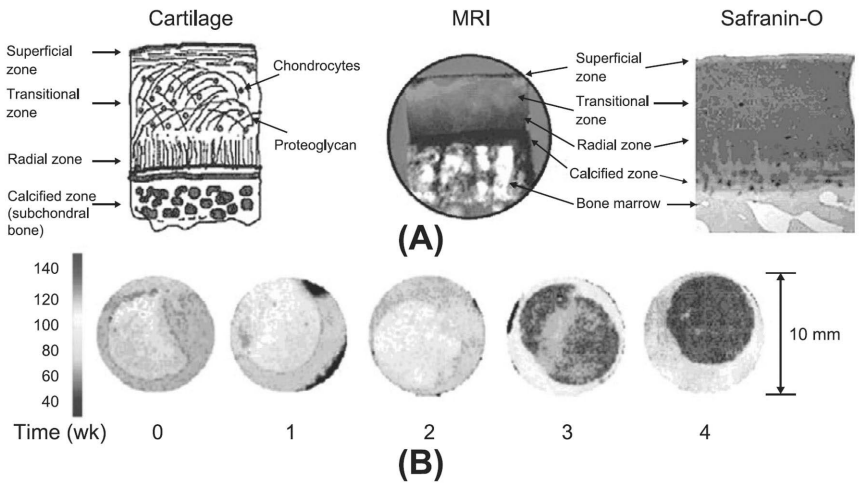

Figure 4. (A) An illustration of the anatomical structure of cartilage along with a high resolution MRI, and a histological image (Safranin-O/Fast green-stained section [40×) of natural cartilage (48). In the MR image, three cartilage zones can be easily identified without contrast agent enhancement. The MR image acquisition parameters are: TR/TE = 1000/60 ms; field-of-view (FOV) = 0.6 cm × 0.6 cm; slice thickness = 0.5 mm; in-plane resolution = 22.7 μm × 22.7 μm; number of averages N = 64. Both the MRI and histological images, depict three layers representing the superficial, transitional, and radial zones. (B) T_2 maps for engineered cartilage over a 4 week growth period. A monotonic increase of T_2 is observed with time in this experiment (Troken, A. J. et al., presented at the annual 2006 BMES Meeting, Chicago, IL, 11–14 Oct. 2006).

cause collagen is recognized by cellular enzymes and naturally degraded (46). Bioreactor systems are also under investigation in cartilage engineering; and an MR-compatible hollow fiber bioreactor system was recently employed for the production and development of three-dimensional hyaline cartilage from isolated chondrocytes (47).

MRI of articular cartilage — High resolution MRI studies are able to distinguish three characteristic zones in articular cartilage: superficial, transitional and radial (for example, see Figure 4). In each zone the MR signal reflects the interactions between water and the distribution of collagen and proteoglycan. Identifying the structure of cartilage via MRI could be an important step in assessing chondrogenesis. As an example, consider the results shown in Figure 4 taken from a study by Othman and coworkers (48). In this figure a comparison is shown between a high resolution 11.7 T MR image of normal articular cartilage and the corresponding tissue histology section stained with safranin O. Over 4 weeks the morphological appearance of developing cartilage in the MR images showed a high correlation with the corresponding histological sections at all stages of development (48). Thus, MRI can be expected to provide useful images for tissue-engineered cartilage.

Progress in monitoring tissue-engineered cartilage *in vitro* — The first step in monitoring tissue-engineered cartilage is to quantify cell growth and tissue development *in vitro*. Studies by Chen and associates (11), Greco and Spencer (49) and Potter and coworkers (47, 50) used 9.4 T MRI to monitor hyaline cartilage growth in a hollow fiber bioreactor (HFBR). All these researchers found a strong correlation between biochemical markers (e.g., tissue cellularity and extracellular matrix composition) and MR parameters (e.g., MTR, T_1, T_2, and ADC). A novel feature of these studies was the use of a specially designed MR compatible bioreactor such that chondrocytes growing inside the HFBR could be monitored periodically over a period of weeks. Water content (via T_1 and T_2) and two main components of the cartilage matrix, namely proteoglycans (via Gd-DTPA enhanced imaging) and collagen (via MTR), were assayed. For example, the average T_2 value decreased from 60 ± 4 ms at week 1 to 35 ± 5 ms at week 4; values comparable with those obtained at the same field strength for natural articular cartilage by Nieminen and coworkers (51). In addition, the measured MTR value at week 1 was similar to that measured for a control collagen gel, while the MTR value measured at week 4 was close to the value reported in the literature for bovine articular cartilage (52). In the study by Potter and coworkers (50), tissue heterogeneity was observed in both the MTR and T_2 data while such heterogeneity is not seen in normal articular cartilage (51). Thus, the MR measurements were able to identify poor tissue development. It should also be noted that electron spin resonance (ESR) has been used by Spencer's group to monitor oxygen consumption in cartilage growing in a HFBR (53). Further studies by Neves and coworkers (54) used MR microscopy and MR spectroscopy at 9.4 T to examine the growth of bioartificial meniscal cartilage tissue *in vitro* in a perfusion bioreactor. Cell-seeding density, medium selection including growth factors, and the application of physical stimuli, such as pressure and flow-induced shear stress, were manipulated to develop meniscal cartilages with properties approaching those of the native tissue. For example, the diffusion into cartilage of the MR paramagnetic contrast agent Gd-DTPA from the medium was used to assess the integrity of the developing zones (54). In this study a diffusion coefficient of 7×10^{-11} m^2/s was reported for Gd-DTPA, which is similar to the 9.2×10^{-11} m^2/s value measured by Foy and Blake in natural human articular cartilage (55).

Recent *in vitro* studies (56, 57) of MSCs embedded in gelatin and chondrocytes embedded in hydrogels used T_2 maps and changes in the apparent water diffusion coefficient to characterize the development of engineered cartilage. An example of the changes in T_2 observed is shown in Figure 4 (Troken, A. J. et al., presented at the annual 2006 BMES Meet-

ing, Chicago, IL, 11–14 Oct. 2006). These data illustrate the successful use of MRI to monitor implant growth and integration with host cartilage.

Progress in monitoring tissue-engineered cartilage *in vivo* — MRI techniques have also been used *in vivo* to characterize the development of tissue engineered cartilage (58], [59, 60). In a study by Watrin-Pinzano and coworkers (58), MR was used to generate T_2 maps during the repair of a focal patellar cartilage defect in a rat. In this study, alginate scaffolds, with and without autologous chondrocytes, were implanted at day 0 to repair rat patellar cartilage defects. The rats were sacrificed sequentially (days 20, 40, and 60) after surgery, and the patellae cartilage samples examined ex-vivo using MRI at 8.5 T. The T_2 values derived from the MR images were found to discriminate between the different types of neo-cartilage; a result confirmed by histological analysis. In a related multinuclear NMR and MRI study by Keinan-Adamsky and associates (59) at 8.5 T using a pig model, the authors found that the order and the density of collagen fibers in articular cartilage increased from birth to maturity. This conclusion was derived from the bi-exponential nature of T_2 relaxation in mature cartilage, as well as its orientational dependence derived from NMR spectral splittings (59). Finally, a recent study by Ramaswamy and coworkers (60, 61) used T_2 relaxation data to assess the regrowth of cartilage in full-thickness chondral defects (surgically created) in rabbits. These studies demonstrate how NMR spectroscopic measurements T_2 relaxation and MRI can be used to obtain structural and compositional information that contributes to a better understanding of the development of natural cartilage.

Adipose Tissue Engineering

Soft tissue defects also present challenges to the tissue engineers. In 2006, breast cancer was the third leading cause of death in American women after heart disease and lung cancer; the cost of this disease was estimated to be over two hundred billion dollars a year in 2005 (62). Breast cancer and other cancers associated with adipose tissue leave patients disfigured following surgery and X-ray treatment; therefore, soft tissue reconstruction is an important clinical concern. In addition to cancer patients, trauma patients undergoing reconstructive surgery could also benefit from improved soft tissue reconstruction procedures.

Adipose tissue is a specialized connective tissue that serves three functions: thermal insulation, energy regulation and mechanical cushioning. The major component of white adipose tissue is a loose association of lipid-filled cells (adipocytes), which are held in a framework of collagen fibers. Approximately 70% of the weight of white adipose tissue is lipid, with over 90% of the lipid in the form of triglycerides. Compared with other mesenchymal tissues, adipose tissue is less stiff and very heterogeneous.

Adipose tissue engineering via an autologous graft is the technique preferred by clinicians. Such grafts are immune compatible and convenient, but they require a donor site, typically from the patient's abdomen. Allogenic or xenogenic grafts are also used in cases where there is the limited availability of autologous grafts. However, one major disadvantage of allogenic and xenogenic grafts is possible immune rejection. Other strategies used for soft tissue reconstruction include the insertion of synthetic materials (for example, silicone, saline bags), but such implants sometimes leak, degrade, or generate a foreign-material reaction (63).

Stem cell-based soft tissue engineering is currently under investigation as an alternative grafting procedure (39). Adipose tissue is one of the types of connective tissue that can be derived from MSCs (64). In this approach, MSCs are seeded into the scaffold to establish a three-dimensional engineered construct that provides a solid framework to simulate the extracellular matrix for cell attachment and proliferation. The engineered cell-scaffold complexes are usually incubated in a supportive physical and mechanical environment that also provides essential nutrients, growth factors and tissue differentiation reagents (65). Current adipose tissue reconstruction has the limitation that it is difficult to monitor graft growth and development. As in the case of tissue engineered bone and cartilage, adipose tissue development is hindered by the absence of non-invasive imaging methods. MRI, which has the capability of distinguishing between the hydrogen atoms in lipids and those in water, is a tool that could be used to monitor adipose tissue regrowth.

MRI of adipose tissue — Adipose tissue is a loose association of lipid-filled cells (adipocytes), which are held in a framework of collagen fibers. Even though adipose tissue is relatively simple in structure, it is challenging to image using MRI. The lipid and water protons behave as if they are located in two different compartments, each with a different resonance frequency: water and lipid proton resonance differs by 225 Hz at 1.5 T. In addition, the protons in lipid and water have separate relaxation times with the lipid protons relaxing via T_1 and T_2 much faster than the water protons. However, these differences in frequency and relaxation times can be used to generate fat suppressed or water and fat suppressed images where the lipid image is generally discarded (66).

Progress in monitoring tissue-engineered fat *in vitro* — MR microscopy at 9.4 T with and without fat suppression was used in a study by Potter and associates (20) to analyze the fat component of tissue-engineered phalanges. The fractional change in the image intensity was used to establish the spatial distribution of mobile lipid molecules within the phalange constructs. Quantitative maps indicating adipose components were acquired 10 and 38 weeks after implantation; the fat deposits observed at week 38 were similar to those observed in histological sections. In a tissue engineering study by Marion and coworkers (Marion, N. et al., presented at the annual 2006 BMES Meeting, Chicago, IL, 11–14 Oct. 2006) the growth stages of engineered fat were monitored using MR measurements of relaxation times and the water diffusion coefficient. In this study of MSC derived adipogenic cells the T_2 values stayed unchanged for 4 weeks, but MR elastography measurements of the bulk modulus showed a significant decrease (Figure 5). By week 4, for example, the shear modulus had decreased to less than one fourth of the initial value (5.8 kPa to 1.4 kPa). The decrease in shear stiffness indicates that the engineered adipogenic tissue becomes "softer" as adipogenic matrix production gradually increases. These results illustrate the complementary role of MRI and MR elastography in assessing the development of engineered tissue *in vitro*.

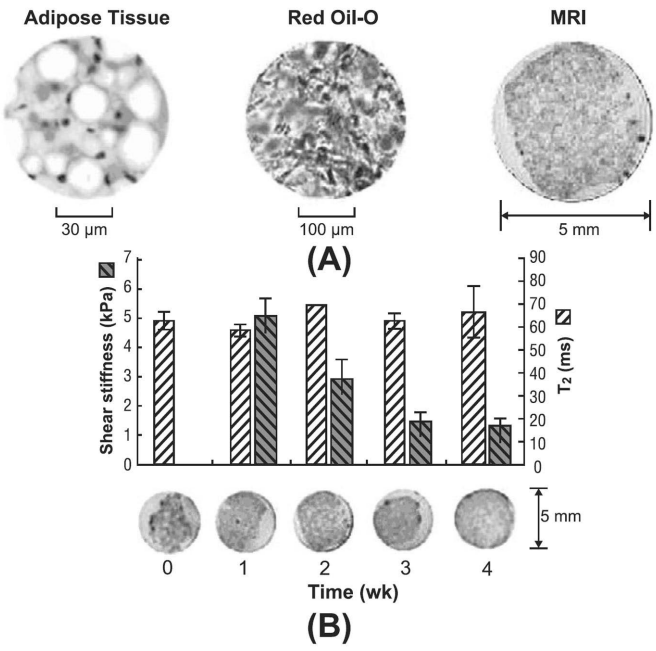

Figure 5. (A) A comparison of histological and MR images of natural fat and an MR image of engineered fat. For the engineered fat, the cells were stained for oil red-O to indicate lipid synthesis as red and counterstained with hematoxylin to mark nuclei blue (25). (B) T_2 relaxation time and shear stiffness data for engineered fat. Although the MR images and T_2 measurements were not able to differentiate between the stages of adipogenesis, the elastography data showed a reduction in stiffness suggesting lipid formation. All data are represented by average ± std (sample size $n = 3$).

Conclusions and Suggested Future Studies

Advances in tissue engineering will rely on improvements at all stages of the tissue development process: choosing the cell source, selecting a biological scaffold, and designing the incubation system. Imaging techniques (for example, optical imaging, MRI, and micro-CT) are important tools for assessing tissue regeneration at each stage of growth. Selection of the most appropriate imaging method depends on several factors: the achievable signal-to-noise ratio, the needed resolution, the presence or generation of contrast, and the desire to visualize tissue structure in a non-invasive manner. Ideally, imaging should provide the tissue engineer with complete information on tissue composition, structure, and function. Realistically, no single imaging modality can do all three. Light microscopy, for example, has the highest resolution but requires tissue sampling, sectioning, and staining, whereas micro-CT is excellent at identifying tissue calcification and bone growth, but has relatively poor soft tissue contrast, while MRI has the highest sensitivity for visualizing soft tissue, but it is technically difficult, expensive and relatively slow in acquiring high resolution images.

MRI, however, does provide a flexible, safe and non-invasive way of measuring many parameters associated with the structural, biochemical and functional changes that occur in developing tissues. A schematic diagram illustrating the connection between tissue growth, tissue properties, and different MR-derived parameters is shown in Figure 6. Since tissue growth and development change the local environment of the tissue water we need to observe these changes over hours, days and weeks as the constructs develop into mature tissues.

MRI has the capability of visualizing tissue development both during the initial *in vitro* stages of cell culture and scaffold incubation and subsequently during tissue implantation development *in vivo*, where the final integration of the implant—its structure and function—with surrounding tissues must be monitored. In the early proliferation stages either the incubator or bioreactor, must be brought to the MRI or the individual constructs must be removed from the incubator to be imaged. Both steps have associated technical problems that are not fully resolved. For example, in the seeding step, the growth of cells in the scaffold must be optimized, and the porosity and diffusion of water in the scaffold need to be examined periodically. This requires sequential MR measurements. In addition, during tissue growth and development, the compartmentalization of tissue water changes; such changes alter the degree of hydration, and can be visualized using MRI and quantified by MR-derived measurements. In the case of engineered bone, for example, water molecules become immobilized at charged surfaces, reducing T_1, while mineral deposition establishes local regions of solid bone altering the local magnetic susceptibility, reducing T_2. For engineered cartilage, collagen and proteoglycan deposition can be quantified by observing changes in the diffusion coefficient and MT values. In both cases, the integration of tissue-engineered constructs with the host tissue *in vivo* needs to be evaluated and the strength and stiffness of the implants assessed by MR elastography. Post-implant monitoring using MRI is crucial to ensure that the engineered constructs and regenerated tissues are functioning normally along with the host tissue.

MRI is also capable of assessing changes in the shape and size of the constructs that often occur during tissue development. Such changes likely reflect normal growth consolidation but they could also be due to non-uniform cell seeding in the scaffold. Since cell seeding density is highly correlated with tissue development, better control of this process is needed. This problem has been recognized by tissue engineers, as they work toward engineering tissues that retain a pre-defined shape. In a similar manner MRI can be used to identify and monitor the development of tissue structures such as the internal layers of articular cartilage and the anisotropy of diffusion in cartilage and muscle.

Finally *in vivo* monitoring of the transitional region between implants and the surrounding tissues is an active area of current research in tissue engineering and regenerative medicine. New high resolution MRI protocols for assessing cell proliferation in tissue engineering are a complement to established optical and micro-CT methods. In the future, improved MR system capabilities should allow NMR spectroscopy and MRI to play an increasing role in tissue engineering, and ultimately speed the development of regenerative medicine as an emerging clinical technique.

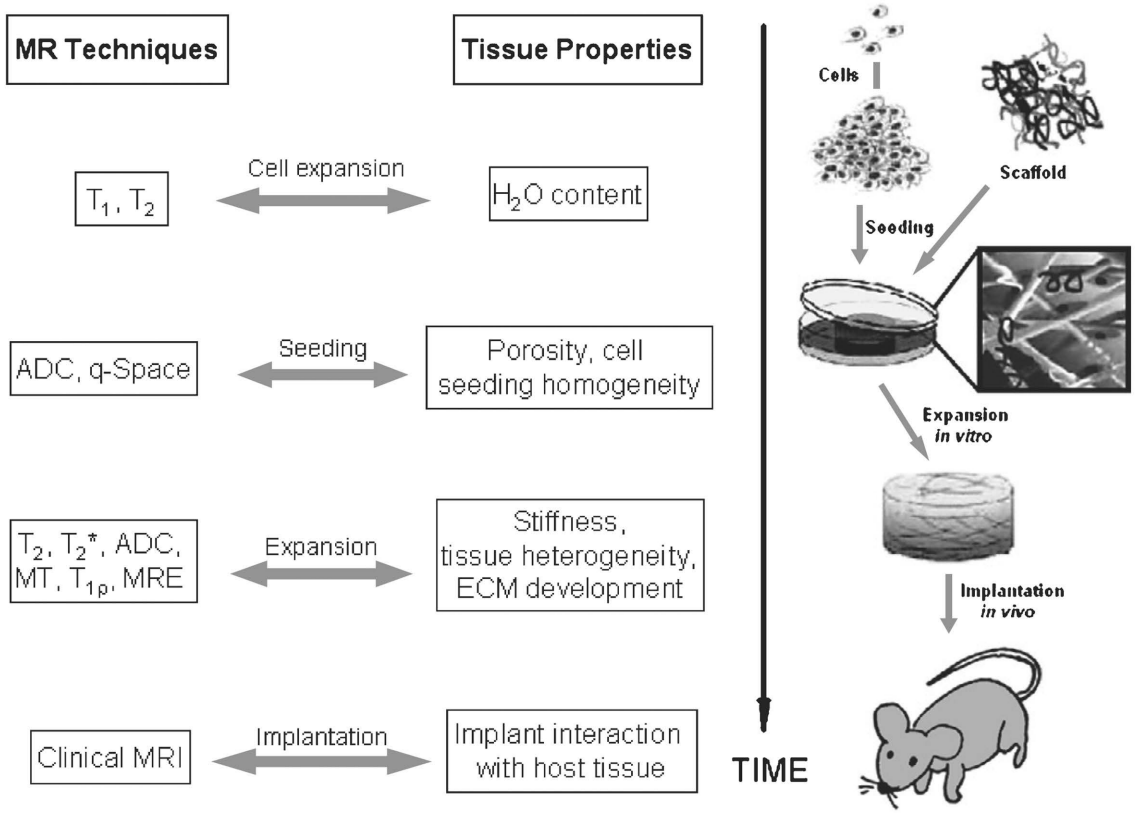

Figure 6. Schematic description of the process of tissue engineering with the correspondence between MR techniques and tissue properties identified at each growth stage.

Acknowledgments — The authors wish to thank the following colleagues for their assistance in preparing this paper: Dr. Liu Hong, Department of Orthodontics, College of Dentistry at the University of Illinois at Chicago, Dr. Robert A. Kleps, Director at the NMR Research Service Facility of the Research Resources Center at the University of Illinois at Chicago, Dr. Jeremy Mao, Department of Orthodontics at Columbia University, and Dr. Carol Muehleman, Department of Biochemistry at Rush University. We also gratefully acknowledge editorial assistance provided by Ms. Lynne Magin, Ms. Evelyn Esquivel and Mr. Lukasz Zientara.

References

1 M. J. Lysaght and J. A. O'Loughlin, Demographic scope and economic magnitude of contemporary organ replacement therapies, *ASAIO J* **46** (2000), pp. 515–521.

2 F. Helmchen and W. Denk, Deep tissue two-photon microscopy, *Nat Methods* **2** (2005), pp. 932–940.

3 A. B. Wolbarst, *Physics of radiology*, Medical Physics Publishing, Madison, WI (1993).

4 L. G. Griffith and G. Naughton, Tissue engineering—current challenges and expanding opportunities, *Science* **295** (2002), pp. 1009–1014.

5 W. S. Pietrzak, *Musculoskeletal tissue regeneration: biological materials and methods*, Humana Press, Totowa, NJ (2008).

6 M. Kino-oka, Y. Maeda, T. Yamamoto, K. Sugawara and M. Taya, A kinetic modeling of chondrocyte culture for manufacture of tissue-engineered cartilage, *J. Biosci. Bioeng.* **99** (2005), pp. 197–207.

7 Y. Irie, H. Mizumoto, S. Fujino and T. Kajiwara, Reconstruction of cartilage tissue using scaffold-free organoid culture technique, *J. Biosci. Bioeng.* **105** (2008), pp. 450–453.

8 J. S. Temenoff and A. G. Mikos, Review: tissue engineering for regeneration of articular cartilage, *Biomaterials* **21** (2000), pp. 431–440.

9 P. Bianco and P. G. Robey, Stem cells in tissue engineering, *Nature* **414** (2001), pp. 118–121.

10 L. L. Hench and J. M. Polak, Third-generation biomedical materials, *Science* **295** (2002), pp. 1014–1017.

11 C. T. Chen, K. W. Fishbein, P. A. Torzilli, A. Hilger, R. G. S. Spencer and W. E. Horton, Matrix fixed-charge density as determined by magnetic resonance microscopy of bioreactor-derived hyaline cartilage correlates with biochemical and biomechanical properties, *Arthritis Rheum.* **48** (2003), pp. 1047–1056.

12 D. D. Stark and W. G. Bradley, *Magnetic resonance imaging* (3rd ed.), Mosby-Year Books, St. Louis (1999).

13 V Kuperman, *Magnetic resonance imaging: physical principles and applications*, Academic Press, San Diego (2000).

14 X. Hu and D. G. Norris, Advances in high-field magnetic resonance imaging, *Annu. Rev. Biomed. Eng.* **6** (2004), pp. 157–184.

15 I. K. Ko, H. T. Song, E. J. Cho, E. S. Lee, Y. M. Huh and J. S. Suh, *In vivo* MR imaging of tissue-engineered human mesenchymal stem cells transplanted to mouse: a preliminary study, *Ann. Biomed. Eng.* **35** (2007), pp. 101–108.

16 P. J. Basser and D. K. Jones, Diffusion-tensor MRI: theory, experimental design and data analysis—a technical review, *NMR Biomed.* **15** (2002), pp. 456–467.

17 S. D. Wolff and R. S. Balaban, Magnetization transfer con-

trast (MTC) and tissue water proton relaxation *in vivo*, *Magn. Reson. Med.* **10** (1989), pp. 135–144.
18 J. R. Wozniak and K. O. Lim, Advances in white matter imaging: a review of in vivo magnetic resonance methodologies and their applicability to the study of development and aging, *Neurosci. Biobehav. Rev.* **30** (2006), pp. 762–774.
19 B. Brochet and V. Dousset, Pathological correlates of magnetization transfer imaging abnormalities in animal models and humans with multiple sclerosis, *Neurology* **53** (1999), pp. S12–S17.
20 K. Potter, D. E. Sweet, P. Anderson, G. R. Davis, N. Isogai, S. Asamura, H. Kusuhara and W. J. Landis, Non-destructive studies of tissue-engineered phalanges by magnetic resonance microscopy and X-ray microtomography, *Bone* **38** (2006), pp. 350–358.
21 U. Duvvuri, S. R. Charagundla, S. B. Kudchodkar, J. H. Kaufman, J. B. Kneeland, R. Rizi, J. S. Leigh and R. Reddy, Human knee: *in vivo* T1rho-weighted MR imaging at 1. 5 T—preliminary experience, *Radiology* **220** (2001), pp. 822–826.
22 U. Duvvuri, R. Reddy, S. D. Patel, J. H. Kaufman, J. B. Kneeland and J. S. Leigh, T1rho-relaxation in articular cartilage: effects of enzymatic degradation, *Magn. Reson. Med.* **38** (1997), pp. 863–867.
23 K. Kuroda, K. Oshio, R. V. Mulkern and F. A. Jolesz, Optimization of chemical shift selective suppression of fat, *Magn. Reson. Med.* **40** (1998), pp. 505–510.
24 R. Muthupillai, P. J. Rossman, D. J. Lomas, J. F. Greenleaf, S. J. Riederer and R. L. Ehman, Magnetic resonance imaging of transverse acoustic strain waves, *Magn. Reson. Med.* **36** (1996), pp. 266–274.
25 Y. Y. Cheung, M. Doyley, T. B. Miller, F. Kennedy, F. Lynch, J. S. Wrobel, K. Paulson and J. Weaver, Magnetic resonance elastography of the plantar fat pads preliminary study in diabetic patients and asymptomatic volunteers, *J. Comput. Assist. Tomogr.* **30** (2006), pp. 321–326.
26 C. T. Laurencin, A. M. A. Ambrosio, M. D. Borden and J. A. Cooper, Tissue engineering: orthopedic applications, *Annu. Rev. Biomed. Eng.* **1** (1999), pp. 19–46.
27 C. T. Laurencin, Y. Khan and S. F. El-Amin, Bone graft substitutes, *Expert Rev. Med. Devices* **3** (2006), pp. 49–57.
28 A. J. Salgado, O. P. Coutinho and R. L. Reis, Bone tissue engineering: state of the art and future trends, *Macromol. Biosci.* **4** (2004), pp. 743–765.
29 D. J. Tyler, M. D. Robson, R. M. Henkelman, I. R. Young and G. M. Bydder, Magnetic resonance imaging with ultrashort TE (UTE) pulse sequences: technical considerations, *J. Magn. Reson.* **25** (2007), pp. 279–289.
30 G. A. Ladinsky and F. W. Wehrli, Noninvasive assessment of bone microarchitecture by MRI, *Curr. Osteoporos. Rep.* **4** (2006), pp. 140–147.
31 F. W. Wehrli, H. K. Song, P. K. Saha and A. C. Wright, Quantitative MRI for the assessment of bone structure and function, *NMR Biomed.* **19** (2006), pp. 731–764.
32 N. R. Washburn, M. Weir, P. Anderson and K. Potter, Bone formation in polymeric scaffolds evaluated by proton magnetic resonance microscopy and X-ray microtomography, *J. Biomed. Mater. Res.* **69** (2004), pp. 738–747.
33 H. Xu, S. F. Othman, L. Hong, I. A. Peptan and R. L. Magin, Magnetic resonance microscopy for monitoring osteogenesis in tissue-engineered construct *in vitro*, *Phys. Med. Biol.* **51** (2006), pp. 719–732.
34 I. E. Chesnick, F. A. Avallone, R. D. Leapman, W. J. Landis, N. Eidelman and K. Potter, Evaluation of bioreactor-cultivated bone by magnetic resonance microscopy and FTIR microspectroscopy, *Bone* **40** (2007), pp. 904–912.
35 S. F. Othman, H. Xu, T. J. Royston and R. L. Magin, Microscopic magnetic resonance elastography (microMRE), *Magn. Reson. Med.* **54** (2005), pp. 605–614.
36 E. H. M. Hartman, J. A. Pikkemmat, J. W. M. Vehof, A. Heerschap, J. A. Jansen and P. H. M. Spauwen, *In vivo* magnetic resonance imaging explorative study of ectopic bone formation in the rat, *Tissue Eng.* **8** (2002), pp. 1029–1036.
37 A. De Ranieri, A. S. Virdi, S. Kuroda, K. E. Healy, N. J. Hallab and D. R. Sumner, Saline irrigation does not affect bone formation or fixation strength of hydroxyapatite/tricalcium phosphate-coated implants in a rat model, *J. Biomed. Mater. Res. B: Appl. Mater.* **74** (2005), pp. 712–717.
38 V. B. Kraus, Pathogenesis and treatment of osteoarthritis, *Med. Clin. North Am.* **81** (1997), pp. 85–112.
39 J. J. Mao, Stem-cell-driven regeneration of synovial joints, *Biol. Cell* **97** (2005), pp. 289–301.
40 C. J. Wirth and M. Rudert, Techniques of cartilage growth enhancement: a review of the literature, *Arthroscopy* **12** (1996), pp. 300–308.
41 G. Meachim and R. A. Stockwell, The matrix. In: M. A. R. Freeman, Editor, *Adult articular cartilage*, Pitman Medical Publishing, London, UK (1979), pp. 1–50.
42 B. Sharma and J. H. Elisseeff, Engineering structurally organized cartilage and bone tissues, *Ann. Biomed. Eng.* **32** (2004), pp. 148–159.
43 P. Angele, R. Kujat, M. Nerlich, J. Yoo, V. Goldberg and B. Johnstone, Engineering of osteochondral tissue with bone marrow mesenchymal progenitor cells in a derivatized hyaluronan-gelatin composite sponge, *Tissue Eng.* **5** (1999), pp. 545–554.
44 E. J. Caterson, L. J. Nesti, W. J. Li, K. G. Danielson, J. J. Albert, A. R. Vaccaro and R. S. Tuan, Three-dimensional cartilage formation by bone marrow-derived cells seeded in polylactide/alginate amalgam, *J. Biomed. Mater. Res.* **57** (2001), pp. 394–403.
45 K. H. Bouhadir, K. Y. Lee, E. Alsberg, K. L. Damn, K. W. Anderson and D. J. Mooney, Degradation of partially oxidized alginate and its potential application for tissue engineering, *Biotechnol. Prog.* **17** (2001), pp. 945–950.
46 D. P. Speer, M. Chvapil, R. G. Volz and M. D. Holmes, Enhancement of healing in osteochondral defects by collagen sponge implants, *Clin. Orthop. Rel. Res.* **144** (1979), pp. 326–335.
47 K. Potter, J. J. Butler, C. Adams, K. W. Fishbein, E. W. McFarland, W. E. Horton and R. G. S. Spencer, Cartilage formation in a hollow fiber bioreactor studied by proton magnetic resonance microscopy, *Matrix Biol.* **17** (1998), pp. 513–523.
48 S. F. Othman, J. Li, O. Abdullah, J. Moinness, R. L. Magin and C. Muehleman, High resolution/High contrast MRI of human articular cartilage lesions, *Acta Orthop.* **78** (2007), pp. 536–546.
49 J. B. Greco and R. G. S. Spencer, Cartilage growth in magnetic resonance microscopy—compatible hollow fiber bioreactors. In: J. B. Chaudhuri and M. Al-Rubeai, Editors, *Bioreactors for tissue engineering*, Kluwer Academic Publishers, The Netherlands (2005), pp. 79–107.
50 K. Potter, J. J. Butler, W. E. Horton and R. G. Spencer, Re-

sponse of engineered cartilage tissue to biochemical agents as studied by proton magnetic resonance microscopy, *Arthritis Rheum.* **43** (2000), pp. 1580–1590.

51 M. T. Nieminen, J. Rieppo, J. Toyras, J. M. Hakumaki, J. Silvennoinen, M. M. Hyttinen, H. J. Helminen and J. S. Jurvelin, T_2 Relaxation time reveals spatial collagen architecture in articular cartilage: a comparative quantitative MRI and polarized light microscopic study, *Magn. Reson. Med.* **46** (2001), pp. 487–493.

52 M. L. Gray, D. Burstein, L. M. Lesperance and L. Gehrke, Magnetization transfer in cartilage and its constituent macromolecules, *Magn. Reson. Med.* **34** (1995), pp. 319–325.

53 S. J. Ellis, M. Velayutham, S. S. Velan, E. F. Peterson, J. L. Zweier, P. Kuppusamy and R. G. S. Spencer, EPR oxygen mapping of engineered cartilage grown in a hollow-fiber bioreactor, *Magn. Reson. Med.* **46** (2001), pp. 819–826.

54 A. A. Neves, N. Medcalf, M. Smith and K. M. Brindle, Evaluation of engineered meniscal cartilage constructs based on different scaffold geometries using magnetic resonance imaging and spectroscopy, *Tissue Eng.* **12** (2006), pp. 53–62.

55 B. D. Foy and J. Blake, Diffusion of paramagnetically labeled proteins in cartilage: enhancement of the 1-D NMR imaging technique, *J. Magn. Reson.* **148** (2001), pp. 126–134.

56 S. Ramaswamy, D. A. Wang, K. W. Fishbein, J. H. Elisseeff and R. G. S. Spencer, An analysis of the integration between articular cartilage and nondegradable hydrogel using magnetic resonance imaging, *J. Biomed. Mater. Res. B. Appl. Biomater.* **77** (2006), pp. 144–148.

57 S. Miyata, T. Numano, K. Homma and T. Ushida, Feasibility of noninvasive evaluation of biophysical properties of tissue-engineered cartilage by using quantitative MRI, *J. Biomech.* **40** (2007), pp. 2990–2998.

58 A. Watrin-Pinzano, J. P. Ruaud, Y. Cheli, P. Gonord, L. Grossin, I. Bettembourg-Brault, P. Gillet, E. Payan, G. Guillot, P. Netter and D. Loeuille, Evaluation of cartilage repair tissue after biomaterial implantation in rat patella by using T_2 mapping, *MAGMA* **17** (2004), pp. 219–228.

59 K. Keinan-Adamsky, H. Shinar and G. Navon, Multinuclear NMR and MRI studies of the maturation of pig articular cartilage, *Magn. Reson. Med.* **55** (2006), pp. 532–540.

60 S. Ramaswamy, I. Gurkan, B. Sharma, B. Cascio, K. W. Fishbein and R. G. Spencer, Assessment of tissue repair in full thickness chondral defects in the rabbit using magnetic resonance imaging transverse relaxation measurements, *J. Biomed. Mater. Res. B: Appl. Biomater.* **86** (2008), pp. 375–380.

61 S. Ramaswamy, D. A. Wang, K. W. Fishbein, J. H. Elisseeff and R. G. Spencer, An analysis of the integration between articular cartilage and nondegradable hydrogel using magnetic resonance imaging, *J. Biomed. Mater. Res. B: Appl. Biomater.* **77** (2006), pp. 144–148.

62 S. Perry, T. L. Kowalski and C. H. Chang, Quality of life assessment in women with breast cancer: benefits, acceptability and utilization, *Health Qual. Life Outcomes* **5** (2007), pp. 24–38.

63 E. A. Ojo-Amaize, M. S. Agopian and J. B. Peter, Novel *in vitro* method for identification of individuals at risk for beryllium hypersensitivity, *Clin. Diagn. Lab Immunol.* **1** (1994), pp. 164–171.

64 A. I. Caplan, Mesenchymal stem cells: cell-based reconstructive therapy in orthopedics, *Tissue Eng.* **11** (2005), pp. 1198–1211.

65 L. Hong, I. A. Peptan, P. Clark and J. J. Mao, *Ex vivo* adipose tissue engineering by human mesenchymal stem cell seeded gelatin sponge, *Ann. Biomed. Eng.* **33** (2005), pp. 511–517.

66 Q. S. Xiang, Two-point water-fat imaging with partially-opposed-phase (POP) acquisition: an asymmetric Dixon method, *Magn. Reson. Med.* **56** (2006), pp. 572–584.